

Low-dimensional dynamo modelling and symmetry-breaking bifurcations

Reik Donner^a, Norbert Seehafer^a, Miguel A.F. Sanjuán^b, Fred Feudel^{a,*}

^a *Institut für Physik, Universität Potsdam, Am Neuen Palais 10, 14469 Potsdam, Germany*

^b *Nonlinear Dynamics and Chaos Group, Departamento de Matemáticas y Física Aplicadas y Ciencias de la Naturaleza, Universidad Rey Juan Carlos, Tulipán s/n, 28933 Móstoles, Spain*

Received 17 March 2006; received in revised form 30 August 2006; accepted 30 August 2006

Available online 11 October 2006

Communicated by A. Mikhailov

Abstract

Motivated by the successful Karlsruhe dynamo experiment, a relatively low-dimensional dynamo model is proposed. It is based on a strong truncation of the magnetohydrodynamic (MHD) equations with an external forcing of the Roberts type and the requirement that the model system satisfies the symmetries of the full MHD system, so that the first symmetry-breaking bifurcations can be captured. The backbone of the Roberts dynamo is formed by the Roberts flow, a helical mean magnetic field and another part of the magnetic field coupled to these two by triadic mode interactions. A minimum truncation model (MTM) containing only these energetically dominating primary mode triads is fully equivalent to the widely used first-order smoothing approximation. However, it is shown that this approach works only in the limit of small wave numbers of the excited magnetic field or small magnetic Reynolds numbers ($Rm \ll 1$). To obtain dynamo action under more general conditions, secondary mode triads must be taken into account. Altogether a set of six primary and secondary mode types is found to be necessary for an optimum truncation model (OTM), corresponding to a system of 152 ordinary differential equations. In a second step, the OTM is used to study symmetry-breaking bifurcations on its route to chaos, with the Reynolds number or strength of the driving force as the control parameter. A decisive role in this scenario is played by a symmetry of the form of $Z_2 \times S^1$ resulting from the Z_2 reflection symmetry of the magnetic field in the MHD equations in conjunction with a circle symmetry S^1 of the Roberts flow. Under its influence, in a secondary Hopf bifurcation from a circle of steady reflection-symmetric states a time-periodic solution branch of oscillating waves (OW) is generated retaining the reflection symmetry, however in a spatio-temporal manner. Finally, the subsequent bifurcations on the route to chaos are examined.

© 2006 Elsevier B.V. All rights reserved.

Keywords: MHD equations; Symmetry-breaking bifurcations; Oscillating waves; Dynamo theory; Alpha-effect

1. Introduction

The generation of magnetic fields due to the motion of electrically conducting fluids is a well studied phenomenon. Introducing an arbitrary weak seed field, one can observe either a weakening, a conservation or even an amplification of this initial field. In the latter two cases one speaks of a dynamo effect [1–7]. Since the pioneering suggestion of Larmor [8] it is believed to be the physical reason for the occurrence of magnetism in planetary and astrophysical objects found in observations. In the past few years homogeneous dynamos as expected to be working in cosmic bodies were realised in laboratory experiments carried out in Riga (Latvia)

[9–15] and Karlsruhe (Germany) [16–21]. Overviews on dynamo experiments in the laboratory can be found in [22–25].

The mathematical framework of dynamo theory is given in terms of a system of coupled nonlinear partial differential equations. In the case of an incompressible non-relativistic fluid, this set can be reduced to four equations, the resistive magnetohydrodynamic (MHD) equations, containing the Navier–Stokes equation (NSE) and the induction equation as coupled evolutionary equations for the fluid velocity $\vec{u}(\vec{x}, t)$ and the magnetic field $\vec{B}(\vec{x}, t)$ and two additional constraints. In dimensionless form, these equations read:

$$\partial_t \vec{u} + (\vec{u} \cdot \nabla) \vec{u} = Re^{-1} \nabla^2 \vec{u} - \nabla P + (\vec{B} \cdot \nabla) \vec{B} + \vec{f} \quad (1)$$

$$\partial_t \vec{B} + (\vec{u} \cdot \nabla) \vec{B} = Rm^{-1} \nabla^2 \vec{B} + (\vec{B} \cdot \nabla) \vec{u} \quad (2)$$

* Corresponding author. Tel.: +49 331 9771227; fax: +49 331 9771142.
E-mail address: fred@agnld.uni-potsdam.de (F. Feudel).

$$\nabla \cdot \vec{u} = 0, \quad \nabla \cdot \vec{B} = 0. \quad (3)$$

Here, $P = p + \vec{B}^2/2$ includes hydrodynamic (p) and magnetic ($\vec{B}^2/2$) pressure contributions and \vec{f} is the sum of the body forces acting on the fluid. Eqs. (3) impose the incompressibility condition on the fluid and ensure the source-free property of the magnetic field. $Re \sim 1/\nu$ and $Rm \sim 1/\eta$ are the standard kinetic and magnetic Reynolds numbers of a flow with kinematic viscosity ν and magnetic diffusivity η . For simplicity, we consider \vec{f} as externally applied and given and do not include processes generating the forces.

Traditional dynamo theory has been mainly kinematic, considering the linear problem whether a prescribed fluid motion can amplify, or at least prevent from decaying, some weak seed magnetic field, disregarding the equation of motion, Eq. (1). The initial point of this paper is a kinematically dynamo-active flow,

$$\vec{u}_R(x, y) = (\sin x \cos y, -\cos x \sin y, 2 \sin x \sin y), \quad (4)$$

which was first studied by Roberts [26,27] and which will be referred to as the Roberts flow in the following. Here it is used to set up a nonlinear dynamo model in which the back reaction of the magnetic on the velocity field is taken into account in the frame of the full nonlinear MHD equations, Eqs. (1)–(3). For this purpose the external body force in Eq. (1) is specified as

$$\vec{f} = -\nabla^2 \vec{u}_R = 2\vec{u}_R \quad (5)$$

in order to compensate viscous losses and to generate the Roberts flow as a stationary solution of the NSE. Together with a vanishing magnetic field it also forms a solution of Eqs. (1)–(3), which is, in addition, stable for small Reynolds numbers.

It should be noted that in most experimental realisations, as e.g. in the Karlsruhe experiment, the dynamo works with fluid sodium. This gives a magnetic Prandtl number of $Pm = 0.88 \times 10^{-5}$ and leads to the same ratio between the magnetic and viscous diffusion time scales. In performing the accompanying computations one is faced with intrinsic numerical difficulties which cannot be solved hitherto. The work presented here will focus on the case $\nu = \eta$ ($Re = Rm$), i.e., the magnetic Prandtl number is kept fixed at a value of $Pm = \nu/\eta = 1$. This approach may be legitimized by the assumption that the small scales of the velocity field have only little influence on the magnetic field generation in the Roberts dynamo. We wish to note, however, that for the small magnetic Prandtl numbers as typical of liquid metals, the fluid will be in a turbulent state at the onset of dynamo action, implying, e.g., a quadratic dependence of the flow resistance on the mean flow velocity (which is important for experimental devices where the fluid is pumped through ducts), while the dependence is linear for $Pm = 1$. With this choice, there remains Re as the only fundamental control parameter. It represents the bifurcation parameter and governs the onset of the dynamo — though generally, if Rm and Re are different, the magnetic Reynolds number Rm is the natural control parameter for dynamo action, no matter how large Re .

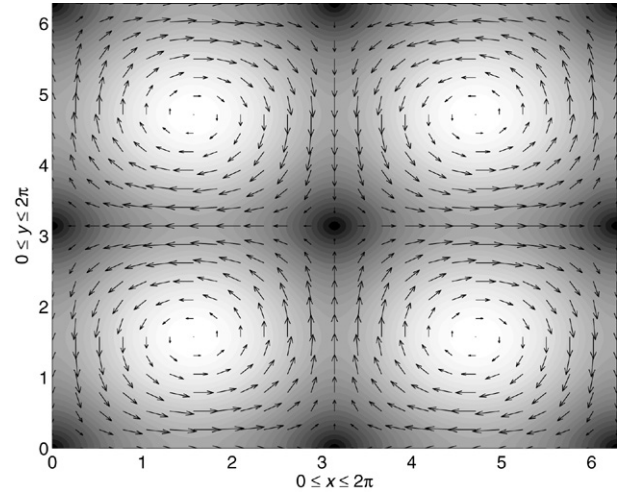


Fig. 1. Projection of the Roberts flow on the x – y plane with arrows indicating the horizontal flow direction. The grey scale measures the modulus of the total velocity where bright areas correspond to high values.

The Roberts flow consists of an array of rolls where the fluid spirals up and down in neighbouring rolls. A projection of the velocity vectors on the x – y plane is plotted in Fig. 1. Since the flow is periodic in the x and y directions, only four rolls are shown. Additionally, it is independent of the z coordinate and thus represents a two-dimensional flow with three non-vanishing components. The roll pattern resembles columnar convection structures in rotating spherical shells [28,29] as have been observed by spacecraft missions in the upper atmospheres of the giant gaseous planets of the solar system [30]. It is believed that roughly similar structures occur as well in the liquid core of the Earth [17]. In this case, these patterns are likely to have a certain relevance for the geodynamo, which is believed to result from convection processes in the planetary interior [5]. This idea motivated the suggestion of a corresponding flow configuration for the design of a dynamo experiment and its subsequent approximate realisation in the Karlsruhe device [16,31–33]. In the meantime, the theory of the dynamo effect in this device has been worked out considerably by using mean-field models and direct numerical simulations of the induction equation, Eq. (2), taking also into account deviations of the actual flow in the experimental device from the Roberts flow [34–45].

The present study continues preceding investigations of the Roberts dynamo where the full nonlinear MHD equations were used [46–48]. In this paper relatively low-dimensional truncation models of the Roberts dynamo are studied. These reduced models allow a clearer identification and better understanding of the basic mode interaction mechanisms. The idea is that essential properties and internal interactions of dynamical systems are often describable by only a few patterns or modes [49–51]. Most of the mean-field studies of the Roberts dynamo mentioned above belong to this category of theoretical description. We show that the minimum truncation model (MTM) we consider here is equivalent to these mean-field models.

However, the main goal of the paper is the derivation of an optimum truncation model (OTM) which, unlike the MTM, is

not restricted to small magnetic Reynolds numbers and works under more general conditions. For this purpose, the modes to be taken into account are chosen on the basis of their energy contributions as computed using the full model. Moreover, it seems advantageous to capture all symmetry properties of the original problem in such a reduced model, so that the symmetry-breaking properties of the bifurcations can be reproduced in a correct manner. The OTM is introduced in Section 2. It is used to study the excitation mechanism of the dynamo with a special regard to the energy transfer from certain basic modes (primary triads) to the other modes. The symmetry-breaking bifurcation that leads from the non-magnetic Roberts flow to a steady-state dynamo solution is described in Section 3. The following bifurcations on the route to chaos are considered in Section 4. Special attention is paid here to the influence of the symmetry breakings on the features of the time-dependent dynamo solutions, as, e.g., oscillating waves (OW). In Section 5, the steady-state Roberts dynamo is discussed by means of an analytical mean-field approach. It is observed that the MTM, containing only the primary mode triads, corresponds to the first-order smoothing approximation of mean-field theory. The critical magnetic Reynolds number for the onset of dynamo action in the MTM is determined in dependence on the vertical wave number of the generated magnetic field, showing that dynamo action in the MTM is restricted to small wave numbers, which is confirmed by our numerical results. In Section 6, finally, the results obtained are briefly discussed.

2. Model setup

The Roberts flow, given by Eq. (4), is invariant in the vertical z direction and periodic in the two horizontal directions x and y . We impose periodic boundary conditions in all three spatial directions, with period lengths $L_x = L_y = 2\pi$ in the horizontal directions and a variable period length L_z in the vertical direction. Compared with the flow patterns in the Karlsruhe dynamo experiment or in planetary interiors, the periodicity assumption for the vertical direction is certainly a crude approximation, and even in the horizontal directions these patterns are, due to their finite extent, only quasi-periodic. Hence the chosen model is the simplest one.

According to the periodicity assumption, Fourier series expansions in the form of

$$a(\vec{x}, t) = \sum_{\vec{k} \neq \vec{0}} a_{\vec{k}} e^{i\vec{k} \cdot \vec{x}}, \quad (6)$$

are used, where $a(\vec{x}, t)$ stands for any of the dynamical variables and the wave vectors \vec{k} are connected with the mode number vectors $\vec{m} = (m_x, m_y, m_z)$, with $m_x, m_y, m_z \in \mathbb{Z}$, by $k_x = 2\pi m_x / L_x$, $k_y = 2\pi m_y / L_y$, $k_z = 2\pi m_z / L_z$. In general, we shall identify the modes by their mode number vectors \vec{m} . In contrast to the preceding studies [46,47], where pseudo-spectral methods were used in the numerics, we now apply a pure spectral method, i.e., all calculations are carried out in Fourier space, so that aliasing errors are completely avoided and actually just the modes selected (see below) are involved in the dynamics of the model system. In accordance with

Eqs. (3), which take the forms $\vec{u}_{\vec{k}} \cdot \vec{k} = 0$ and $\vec{B}_{\vec{k}} \cdot \vec{k} = 0$ in Fourier space, $\vec{u}_{\vec{k}}$ and $\vec{B}_{\vec{k}}$ are projected onto the plane perpendicular to \vec{k} , resulting in an infinite-dimensional system of ordinary differential equations for the transverse parts of $\vec{u}_{\vec{k}}$ and $\vec{B}_{\vec{k}}$, with the pressure eliminated. For details see Appendix A.

Several details of the bifurcation scenario of the dynamical system defined by Eqs. (1)–(5) were explored in [46,47]. The consequent use of a Fourier representation with a truncation at $|m_x|, |m_y|, |m_z| = 8$ leads to a system of 16 384 coupled ordinary differential equations of first order for the real and imaginary parts of the complex Fourier coefficients of the velocity and magnetic field. Calculations using such a high number of variables are impractical in detailed bifurcation and mode interaction studies if the dynamics of the physical system is essentially controlled by only a few dominating modes.

To check out whether the latter is the case for the Roberts dynamo, the kinetic and magnetic energy distributions

$$E_{\text{kin}}(\vec{k}) = \frac{|\vec{u}_{\vec{k}}|^2}{2}, \quad E_{\text{mag}}(\vec{k}) = \frac{|\vec{B}_{\vec{k}}|^2}{2} \quad (7)$$

over the different Fourier modes have been examined. Besides the general decrease of the amount of energy per mode with increasing $|\vec{k}|$, it turns out that for the steady-state Roberts dynamo, i.e., for the primary dynamo solution bifurcating from the nonmagnetic Roberts flow, there is indeed a distinctive energy hierarchy of the Fourier modes where only a small number of modes is significantly excited kinetically or magnetically and the energy per mode drops strongly towards the rest of the (non-vanishing) modes.

For deriving a model system by truncating the full system, the symmetries of the problem are most important and have thus to be retained. The symmetries of the Roberts flow were analysed in Ref. [47] and are briefly summarised here. With our periodic boundary conditions, the invariance of the Roberts flow and, thus, the invariance of the MHD equations with Roberts forcing, Eqs. (1)–(5), with respect to translations in the z direction is described by the circle group S^1 . Furthermore, the system of Eqs. (1)–(5) possesses a discrete symmetry group including a subgroup $G = Z_4 \times_S D_2$, the semidirect product of the cyclic and dihedral groups, representing the geometric structure of the Roberts flow, and the Z_2 invariance $\vec{u} \rightarrow \vec{u}$, $\vec{B} \rightarrow -\vec{B}$ as an intrinsic property of the MHD equations. As found in Ref. [47] for the full system, the discrete symmetry subgroup survives the dynamo bifurcation (though the actions of the corresponding transformations are modified), while the continuous S^1 invariance is broken.

Thus, the reduced model system should exhibit a bifurcation from the original Roberts flow to a dynamo solution that remains invariant with respect to the discrete symmetry group G of the problem. The latter implies that with a given Fourier mode included in the model, also all those modes have to be included which can be obtained from the given mode by one of the discrete symmetry transformations. In this way a whole hierarchy of models, with an increasing number of modes included, can be constructed.

Table 1
Kinetic and magnetic energy per mode type in the stationary dynamo regime of the OTM at the Reynolds number $Re = 3.0$ for the case of periodicity lengths of 2π in all three spatial directions

\vec{k}	E_{kin}	E_{mag}
$(\pm 1, \pm 1, 0)$	5.6005	–
$(0, 0, \pm 1)$	–	0.0482
$(\pm 1, \pm 1, \pm 1)$	–	0.1419
$(0, \pm 2, \pm 1)$	–	0.0204
$(\pm 2, 0, \pm 1)$	–	0.0204
$(\pm 1, \pm 3, \pm 1)$	–	0.0176
$(\pm 3, \pm 1, \pm 1)$	–	0.0176
Total	5.6005	0.2660

Dashes denote vanishing contributions.

Table 1 gives the modes of two models in this hierarchy which are considered in the following. From the kinetic and magnetic energy distributions after the onset of the dynamo listed in the table for the case of period lengths of 2π in all three directions, it is seen that, firstly, in the velocity field only the Fourier modes with mode number vectors $\vec{m}^{(1)} = (\pm 1, \pm 1, 0)$, corresponding to the primary Roberts flow, are excited. Actually the flow is still the Roberts flow, only weakly disturbed in its strength. Secondly, the most energetic bifurcating magnetic modes are those with mode number vectors $\vec{m}^{(2)} = (0, 0, \pm 1)$. These magnetic modes correspond to a horizontally averaged or mean field, cf. Section 3. Along with $\vec{m}^{(1)}$ and $\vec{m}^{(2)}$, the modes with $\vec{m}^{(3)} = (\pm 1, \pm 1, \pm 1)$ have not to be truncated because their mode number vectors \vec{m}^3 are coupled to $\vec{m}^{(1)}$ and $\vec{m}^{(2)}$ by triadic interactions ($\vec{m}^{(3)} = \vec{m}^{(1)} + \vec{m}^{(2)}$). The essential role of these three mode types in the Roberts flow driven dynamo has already been recognised by Busse as described in Refs. [32,35,52] where he used a mean-field approach to the corresponding kinematic problem. These couple of modes, which we call the primary mode triads, form an MTM admitting dynamo solutions. However, as shown in Section 5, it works only in the limit of small vertical wave numbers and the critical magnetic Reynolds number for dynamo action tends to infinity as $k_z \rightarrow 1$. Hence, we looked for a more general model. As a result of systematic investigations, an OTM has been set up which overcomes these limitations. It contains, additionally, the magnetic modes with $\vec{m} = (\pm 2, 0, \pm 1)$, $(0, \pm 2, \pm 1)$ and $\vec{m} = (\pm 3, \pm 1, \pm 1)$, $(\pm 1, \pm 3, \pm 1)$. Together with the velocity modes with $\vec{m} = (\pm 1, \pm 1, 0)$ they form sets of interacting triads that do not contain the primary magnetic modes with $\vec{m} = (0, 0, \pm 1)$ and which, therefore, are called secondary mode triads in the following. In Fig. 2 the interactions of the selected modes are depicted schematically. The modes of the MTM are placed in the central panel of the figure. The arrows denote the way the MTM modes interact with the other modes to form a set of secondary modes triads, the construct of the OTM.

In summary, with this selection of Fourier modes an OTM is obtained which admits dynamo solutions for a wide range of vertical wave numbers. Moreover, it fulfills all symmetry requirements of the steady-state dynamo solution of the full system. Consequently, the Roberts dynamo can be

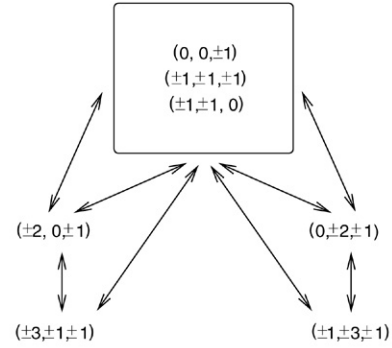


Fig. 2. Schematic representation of the interacting mode triads.

approximately described by an OTM consisting of a system of 19 independent Fourier modes (here the reality condition $a_{-\vec{k}} = a_{\vec{k}}^*$, where an asterisk denotes the complex conjugate, is taken into account). In order to be not too restrictive, in particular to leave enough freedom for the subsequent bifurcations, both the magnetic and the velocity mode coefficients for the Fourier modes with the selected wave numbers are taken into account, which amounts to eight real variables per Fourier mode, cf. Appendix A. This finally gives a system of 152 real differential equations, which will be studied in the following sections.

3. Dynamo excitation

The onset of dynamo action at a critical value of the Reynolds number is caused by the instability of a purely magnetic eigenmode with $k_z = \pm 2\pi/L_z$, i.e. with the largest possible wavelength in the z direction [43,44,46,47,53]. Among the contributions to this eigenmode, the Fourier modes with $\vec{m} = (0, 0, \pm 1)$, corresponding to a horizontally averaged or mean field that rotates without changing its modulus in a spiral-staircase-like fashion about the z axis (cf. Section 5), are most important for the physical mechanism of the Roberts dynamo [27,54–56]. Because of $\nabla \cdot \vec{B} = 0$ this mean field is purely horizontal. Actually there is no dynamo effect up to high values of Rm if the modes with $\vec{m} = (0, 0, \pm 1)$ are explicitly excluded. The horizontal mean field is both decisive for the mechanism of the Roberts dynamo and energetically dominating. Its energetic dominance has been confirmed in the Karlsruhe dynamo experiment [17,18].

In the following a bifurcation analysis of the OTM to Eqs. (1)–(3) is performed for the special case of equal periodicity lengths $L_x = L_y = L_z = 2\pi$, with the Reynolds number $Re = Rm$ as the relevant control parameter. In a linear stability analysis of the nonmagnetic Roberts flow, it is found that at $Re = 2.61$ two real eigenvalues of the Jacobian matrix pass through zero simultaneously, indicating a degenerate pitchfork bifurcation. This observation correctly reproduces the results of the high-dimensional investigations in [46] where the instability was found at $Re \approx 2.8$ (in the normalisation used in the present paper; the value given in [46] corresponds to a different definition of the Reynolds number). The small shift in the critical parameter value can be explained by a reduced energy dissipation rate due to the

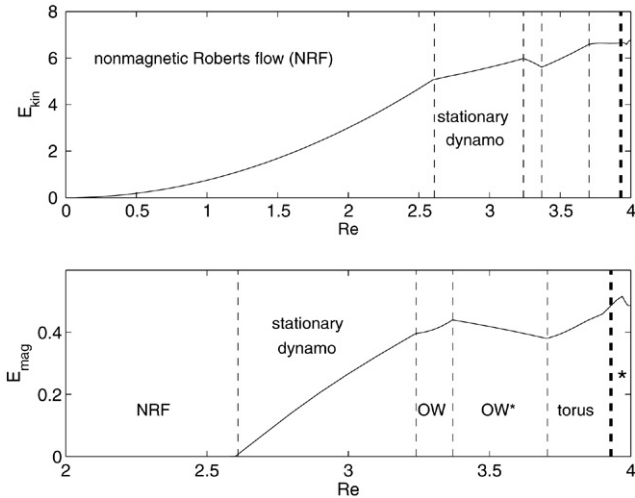


Fig. 3. Bifurcation diagram in the form of the temporal averages of kinetic and magnetic energy as functions of Re . Thin dashed vertical lines indicate transition points between different solution branches. The Hopf bifurcation at $Re = 3.24$ creates oscillating waves (OW). The thick dashed vertical line corresponds to a finite solution branch (see text) and the asterisk denotes the chaotic regime.

missing contributions of the higher modes. The degeneracy (multiplicity two of the eigenvalue) is directly related to the continuous S^1 symmetry of the original Roberts flow in the z direction, which is broken by this bifurcation. The two-dimensional unstable linear eigenspace consists of a continuum of modes where one can be transformed into the other by a z translation. Correspondingly, the bifurcating dynamo branch consists of a continuum of equivalent solutions describing a group orbit. Although the translation symmetry is broken by the generated magnetic field, the flow remains independent of the z coordinate. The magnetic field brakes the Roberts flow by the Lorentz force without changing its functional form, which is indicated in Table 1 by the fact that only the velocity modes with $\vec{m} = (\pm 1, \pm 1, \pm 0)$ are excited. This illustrates the feasibility of a three-dimensional dynamo that is maintained by a two-dimensional velocity field, a situation which is not in conflict with the Cowling theorem [1]. It should be mentioned, however, that in the OTM considered here this phenomenon is a consequence of the strong truncation and that the flow becomes three-dimensional as well when further modes are taken into account.

In Table 1 the contributions to kinetic and magnetic energy of the different mode types, calculated using Eq. (7), are given for the steady-state dynamo at $Re = 3.0$. The modes belonging to the primary triads contain more than 98% of the total energy and more than 70% of the magnetic energy. The forced modes with $\vec{m} = (\pm 1, \pm 1, \pm 0)$, containing all kinetic energy, do not contribute to the magnetic field.

The computed bifurcation diagram is depicted in Fig. 3, presenting the kinetic energy (upper panel) as well as the magnetic energy (lower panel) as functions of the Reynolds number. The vertical lines mark the bifurcation points (note that the horizontal coordinate axes have different scales in the two panels of the figure, but the critical values of course coincide). The first transition line gives the onset of the stationary dynamo.

For the nonmagnetic Roberts flow (NRF), the kinetic energy increases exactly with the square of Re , or to be more precise, $\vec{u} = Re \vec{u}_R$ holds. Due to the magnetic field generation, this increase becomes remarkably weaker after the onset of the dynamo.

The steady-state dynamo preserves the above mentioned Z_2 symmetry of the MHD equations. It has changed its action such that now the reflection $\vec{u} \rightarrow \vec{u}, \vec{B} \rightarrow -\vec{B}$ of the fields has to be combined with an additional shift of the solution by π in the z direction. This, however, is a consequence of the idealisations in our model, namely, the infinite extent of the system and the periodic boundary conditions. Therefore, a comparison with the Karlsruhe dynamo experiment seems in order. In the experiment, dynamo states are observed that are steady on time average, with turbulent fluctuations superposed. There are two steady states with oppositely directed magnetic fields. Their coexistence obviously corresponds to the Z_2 invariance $\vec{u} \rightarrow \vec{u}, \vec{B} \rightarrow -\vec{B}$ of the MHD equations. The two dynamo branches found in the experiment are not fully identical in their stability properties and do not seem to be directly connected. The asymmetry between the two branches can be explained by the presence of the geomagnetic field. Correspondingly, the onset of dynamo action in the experiment has been characterised as an imperfect (pitchfork) bifurcation [21,37,42].

4. Time-dependent dynamo

In addition to the single real zero eigenvalue, representing the group orbit of the steady-state solutions, a pair of complex-conjugate eigenvalues crosses the imaginary axis at $Re \approx 3.24$, indicating a secondary bifurcation (cf. Fig. 3). This bifurcation, after which all modes of the OTM are excited both kinetically and magnetically, corresponds to a symmetry-breaking Hopf bifurcation from a circle of stationary dynamo solutions. The imaginary part of the critical eigenvalues, $\omega \approx 2.2$, is in good agreement with the frequency of the mode coefficients which are newly excited by this bifurcation. They oscillate nearly harmonically with a zero mean value. By contrast, the mode coefficients which were non-vanishing already before the bifurcation start to oscillate with twice the Hopf frequency about their mean values. To demonstrate this feature, Fig. 4 shows, as an example, the time dependence of two selected mode coefficients, $\Re(u_{(1,1,1)}^{(1)})$ and $\Re(B_{(0,0,1)}^{(1)})$ (for the definition of the coefficients see Appendix A; \Re and \Im denote real and imaginary parts).

Obviously this bifurcation is not a simple Hopf bifurcation but it is governed by the symmetry of the equations. Together with the rotational symmetry due to the z independence of the flow, the Z_2 invariance, introduced in Section 2 and also discussed in the preceding section, plays an essential role. Since both groups commute in their action, the direct product $S^1 \times Z_2$ is the relevant group which controls the bifurcation. The situation is very similar, though not identical, to the $O(2)$ symmetry-breaking bifurcations extensively studied in Refs. [57–59]. In both cases the Hopf bifurcation generates wave solutions from a circle of steady states. Landsberg and Knobloch [57] called them direction-reversing travelling

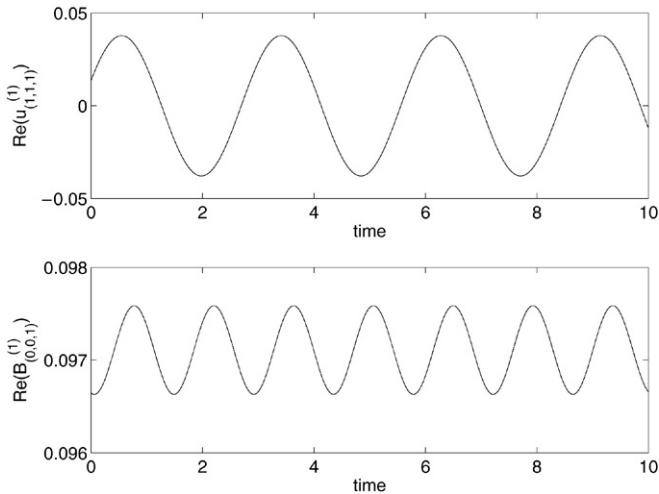


Fig. 4. Oscillations of the mode coefficients $\Re(u_{(1,1,1)}^{(1)})$ (upper panel) and $\Re(B_{(0,0,1)}^{(1)})$ (lower panel) for the solution on the branch OW at $Re = 3.25$ (the mode coefficients are defined by Eqs. (A.1) and (A.2) in Appendix A).

waves. Amdjadi and Gomatam [58] introduced canonical coordinates for the Z_2 symmetric steady-state solutions and showed that the bifurcating periodic orbit preserves a special spatio-temporal symmetry. They called this solution branch oscillating waves (OW) and we follow their terminology. The corresponding solutions are still Z_2 symmetric, however with respect to a spatio-temporal action given by the combination of the reflection $\vec{u} \rightarrow \vec{u}$, $\vec{B} \rightarrow -\vec{B}$ with a translation by π in the z direction and a phase shift by half a period, $T/2$. As a consequence, the modes are either symmetric under a time shift by $T/2$ or they are antisymmetric. The modes already excited in the stationary state before the Hopf bifurcation are symmetric to the spatial part of the transformation without the time shift, while the newly excited ones are lacking this purely

spatial symmetry. Thus, two oscillation frequencies appear in the system and the modes which belong to the symmetric subspace oscillate with twice the Hopf frequency. Albeit in the situation under consideration the $S^1 \times Z_2$ group instead of the $O(2)$ group is the relevant symmetry group, the bifurcating wave solutions have the same properties and we identify them with OW.

The OW represent a special kind of standing oscillation that differs from a standard standing wave. For the latter one, in a plane spanned by any two of the real or imaginary parts of the Fourier coefficients, the system moves periodically on a straight line. In particular, the projections of the system trajectory on the planes spanned by the real and imaginary parts of a given Fourier coefficient are straight lines. For our OW branch, the coefficients of the mean magnetic field, with $m = (0, 0, \pm 1)$, indeed behave in this way, as is seen in upper left panel of Fig. 5, where the projection of the magnetic field on the real and imaginary parts of the mean-field mode coefficient $B_{(0,0,1)}^{(1)}$ is depicted. For all Fourier coefficients not belonging to the mean magnetic field, however, the corresponding projections are ellipses.

The Hopf bifurcation is followed by a tertiary bifurcation at $Re \approx 3.37$, where, as is seen in the bifurcation diagram (Fig. 3), the magnetic energy becomes a decreasing function of the Reynolds number. Interestingly, this bifurcation does not break the above explained spatio-temporal Z_2 symmetry and leaves the system strictly time periodic. The new solution branch, OW*, resembles the branch OW. There is, however, a difference between the two branches in the behaviour of the modes making up the mean magnetic field, with $\vec{m} = (0, 0, \pm 1)$. The mean field $\langle \vec{B} \rangle$ generated in the (primary) dynamo bifurcation is a Beltrami or force-free field, i.e., the mean electric current density, $\langle \vec{j} \rangle = \nabla \times \langle \vec{B} \rangle$, is parallel to $\langle \vec{B} \rangle$ (cf. Section 5). The Beltrami property implies that the modulus of the mean

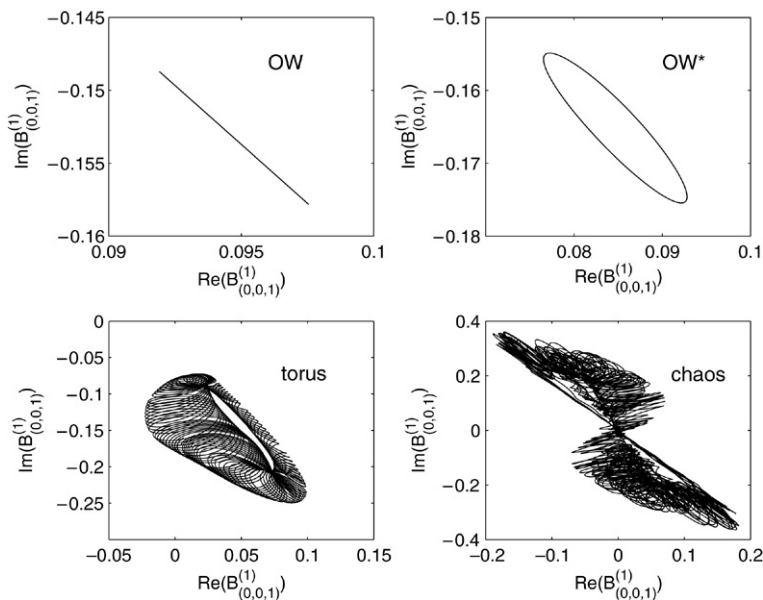


Fig. 5. Projection of the phase space trajectory on the plane spanned by the real and imaginary parts of the mode coefficient $B_{(0,0,1)}^{(1)}$ (defined by Eq. (A.2) in Appendix A) for $Re = 3.3$ (upper left), $Re = 3.4$ (upper right), $Re = 3.8$ (lower left) and $Re = 4.0$ (lower right).

magnetic field is independent of z (the field direction varying as a function of z in a spiral-staircase-like fashion). In the time-periodic regime between the Hopf bifurcation and the tertiary bifurcation at $Re \approx 3.37$, $\langle \vec{B} \rangle$ has still the Beltrami property, oscillating with spatially constant modulus. At $Re \approx 3.37$, the temporal behaviour of the mean-field modes becomes similar to that of the other modes, namely, the projection of the system trajectory on the plane spanned by the real and imaginary parts of $B_{(0,0,1)}^{(i)}$ ($i = 1, 2$) changes from a straight line to an ellipse, as shown in the upper right panel of Fig. 5. In configuration space, the mean magnetic field gets a more inhomogeneous structure. In particular, its modulus now oscillates in both time and space and $\langle \vec{B} \rangle$ is no longer a Beltrami field. Obviously the mean magnetic field changes to a form where it is less easily excited by the Roberts flow (to which the flow is still very close). This can explain the decrease of the magnetic energy starting at $Re \approx 3.37$.

Oscillations were also found in numerical simulations related to the Karlsruhe dynamo experiment by Sarkar and Tilgner [60]. These authors also assumed a periodic geometry and applied an explicit forcing to drive a Roberts type flow. To come closer to the situation in the real experiment, the forcing was only applied inside circular cylinders (four in the periodic horizontal box) and set equal to zero in the rest of the volume. The oscillations already occur in the kinematic regime, which indicates that the primary dynamo bifurcation is a Hopf bifurcation (unlike the steady-state bifurcation that we observe, cf. Section 3), and are characterised by rotations of the magnetic field patterns in each of the cylinders, while the oscillations that we observe (originating in secondary or tertiary bifurcations) are better characterised as pulsations, as described above. A deeper understanding of these differences will require further studies.

In summary, the OW and OW* branches show spatio-temporal features in their dynamics that are essentially determined by the symmetry-breaking properties of the Hopf bifurcation at $Re \approx 3.24$. The original Roberts flow is only slightly modified for these time-periodic branches. Fig. 6 shows snapshots of the vertical velocity component u_z in the plane $x = 0$. In this plane, where $u_z = 0$ for the Roberts flow, the oscillation of the velocity field becomes clearly visible. For instance, u_z has completely reversed its direction after half a period. The changes observed mainly result from deformations of the boundaries between neighbouring rolls where the vertical velocity component changes its sign.

The branch OW* ends up in a further Hopf bifurcation at $Re \approx 3.7$, resulting in a quasiperiodic motion on a torus (lower left panel in Fig. 5). The torus solution remains stable up to $Re \approx 3.90$. At this point the torus loses its asymptotic stability and an additional marginally stable direction appears in the phase space of the system. Computing the largest Lyapunov exponents, one observes that one of the negative Lyapunov exponents becomes zero and remains zero over a small, but finite interval of the Reynolds number, $3.90 \leq Re \leq 3.923$, indicating the additional neutral direction. This solution branch is, thus, characterised by the special feature that four Lyapunov exponents are equal to zero (on the torus branch between

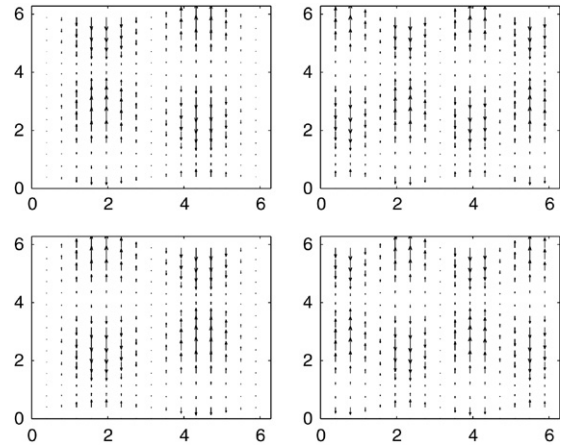


Fig. 6. Snapshots over one period T of the OW at $Re = 3.3$. The arrows show direction and strength of the vertical velocity component u_z in the plane $x = 0$ at times $t = 0.25 T$ (upper left), $t = 0.5 T$ (upper right), $t = 0.75 T$ (lower left) and $t = T$ (lower right). The y and z axes point to the right and upward, respectively.

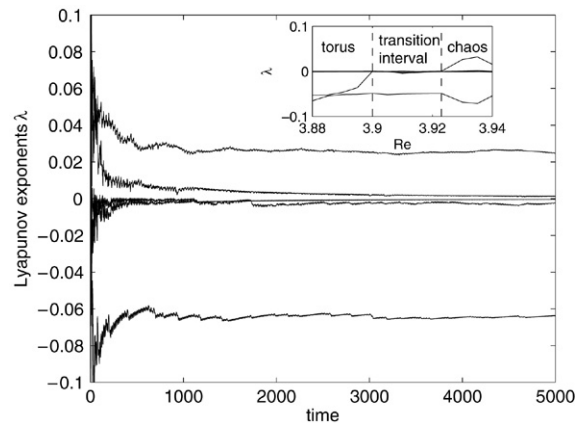


Fig. 7. The five largest Lyapunov exponents versus simulation time after the onset of chaos at $Re = 3.930$. The inset shows the Lyapunov exponents versus Re , demonstrating the existence of the finite transition interval with four vanishing Lyapunov exponents preceding the chaos onset.

$Re \approx 3.7$ and $Re \approx 3.90$, there were three vanishing Lyapunov exponents, two resulting from the torus character of the solution and one from the continuous S^1 invariance of the system). In the bifurcation diagram, Fig. 3, the location of the finite interval where this solution branch is stable is indicated by a thick dashed line. For higher Reynolds numbers then chaos sets in. We suppose that this extraordinary route to chaos is likewise induced by the $S^1 \times Z_2$ symmetry. An example of a chaotic trajectory for $Re = 4.0$, where chaos is already fully developed, is depicted in the lower right panel of Fig. 5. The chaotic nature of the bifurcating branch is proven by computing the six largest Lyapunov exponents, of which one becomes clearly positive. In order to demonstrate the good convergence of the used numerical method, in Fig. 7 the five largest Lyapunov exponents over simulation time are shown for $Re = 3.930$, a value slightly above the chaos onset. The differences between these five Lyapunov exponents are remarkably small in comparison to the sixth calculated exponent, which deviates by more than ten orders of magnitude from them and is, therefore, not shown

in this figure. Nevertheless, one of the Lyapunov exponents is obviously positive while three of them are zero (i.e., three of the finite-time exponents shown in Fig. 7 tend to zero asymptotically in time). In order to make sure the existence of the intermediate branch where four Lyapunov exponents are zero, the inset in Fig. 7 gives the five Lyapunov exponents as functions of Re for this region.

In a summary of this section, we conclude that the $S^1 \times Z_2$ subsymmetry of the system essentially governs the features of the time-dependent dynamo states and leads to a special route to chaos.

5. Mean-field considerations

For the description of dynamo action in a turbulent flow mean-field dynamo theory is often applied [1–4,61]. The central mechanism in this theory is the generation of a mean, or large-scale, electromotive force (emf)

$$\vec{\mathcal{E}} = \langle \vec{u}' \times \vec{B}' \rangle = \vec{\mathcal{E}}_{\parallel} + \vec{\mathcal{E}}_{\perp} = \alpha \langle \vec{B} \rangle + \vec{\mathcal{E}}_{\perp} \quad (8)$$

by turbulently fluctuating, or small-scale, parts of the velocity and magnetic field. Here for a fluctuating quantity \vec{a} , we write $\vec{a} = \langle \vec{a} \rangle + \vec{a}'$, where $\langle \cdot \rangle$ is a suitably defined average. The presence of a non-vanishing component $\vec{\mathcal{E}}_{\parallel} = \alpha \langle \vec{B} \rangle$ of $\vec{\mathcal{E}}$ parallel to the mean magnetic field $\langle \vec{B} \rangle$ is known as the α -effect (slightly different from this definition, which we use here, $\vec{\mathcal{E}}$ is very often expanded as $\mathcal{E}_i = a_{ij} \langle B_j \rangle + b_{ijk} \frac{\partial \langle B_j \rangle}{\partial x_k} + \dots$, which takes the form $\vec{\mathcal{E}} = \tilde{\alpha} \langle \vec{B} \rangle - \beta \nabla \times \langle \vec{B} \rangle + \dots$ in the case of isotropic fluctuations, and the notion of α -effect refers then only to the first term of the expansion, though the second term, which is interpreted as a turbulent diffusivity, may have a component parallel to $\langle \vec{B} \rangle$ as well). The splitting up of the velocity and magnetic fields into mean and fluctuating parts leads to a separation of Eq. (2) into two coupled equations for the temporal evolutions of $\langle \vec{B} \rangle$ and \vec{B}' , namely

$$\partial_t \langle \vec{B} \rangle = \nabla \times (\langle \vec{u} \rangle \times \langle \vec{B} \rangle) + Rm^{-1} \nabla^2 \langle \vec{B} \rangle + \nabla \times \vec{\mathcal{E}}, \quad (9)$$

$$\begin{aligned} \partial_t \vec{B}' &= \nabla \times (\vec{u}' \times \langle \vec{B} \rangle) + \nabla \times (\langle \vec{u} \rangle \times \vec{B}') \\ &\quad + Rm^{-1} \nabla^2 \vec{B}' + \nabla \times \vec{G}, \end{aligned} \quad (10)$$

where

$$\vec{G} = \vec{u}' \times \vec{B}' - \langle \vec{u}' \times \vec{B}' \rangle. \quad (11)$$

Let the mean fields be defined as horizontal averages,

$$\langle \vec{a} \rangle(z) = \frac{1}{L_x L_y} \int_0^{2\pi} \int_0^{2\pi} \vec{a}(x, y, z) dx dy, \quad (12)$$

that is, as the sum of the respective Fourier modes with wave vectors $\vec{k} = (0, 0, k_z)$. For both the high-dimensional and low-dimensional calculations the mean velocity vanishes, while the mean magnetic field is given by (modulo a vertical shift)

$$\langle \vec{B} \rangle(z) = B_0 [\cos(k_0 z), \sin(k_0 z), 0], \quad (13)$$

where $B_0 = |\langle \vec{B} \rangle|$ is independent of the spatial position, i.e., of the z coordinate, but may depend on time. This spiral-staircase-like structure of the mean field is well-known for the kinematic Roberts dynamo and was recently found for the nonlinear case as well [47,62]. Our numerical calculations in Sections 3 and 4 were restricted to the case of $k_0 = 1$, but for the considerations of this section we also admit vertical wave numbers $k_0 \neq 1$ for the magnetic field, corresponding to period lengths of $L_z = 2\pi/k_0$ in the z direction. The horizontal period lengths remain $L_x = L_y = 2\pi$.

From Eq. (13) we get

$$\nabla \times \langle \vec{B} \rangle = -k_0 \langle \vec{B} \rangle, \quad (14)$$

i.e., $\langle \vec{B} \rangle$ is a Beltrami field. With

$$\nabla^2 \langle \vec{B} \rangle = -\nabla \times \nabla \times \langle \vec{B} \rangle = -k_0^2 \langle \vec{B} \rangle, \quad (15)$$

as implied by Eq. (14), and $\langle \vec{u} \rangle = \vec{0}$, Eq. (9) takes the form

$$\partial_t \langle \vec{B} \rangle = -Rm^{-1} k_0^2 \langle \vec{B} \rangle + \nabla \times \vec{\mathcal{E}}, \quad (16)$$

which, using Eq. (13), can be written as

$$\nabla \times \vec{\mathcal{E}} = \left(\frac{k_0^2}{Rm} + \frac{d(\ln B_0(t))}{dt} \right) \langle \vec{B} \rangle. \quad (17)$$

All mean quantities, including $\vec{\mathcal{E}}$, depend only on the z coordinate (and time t). Employing once more the Beltrami property of $\langle \vec{B} \rangle$ expressed by Eq. (14), Eq. (17) can be integrated with respect to z to give

$$\vec{\mathcal{E}} = -\frac{1}{k_0} \left(\frac{k_0^2}{Rm} + \frac{d(\ln B_0(t))}{dt} \right) \langle \vec{B} \rangle + \mathcal{E}_z(z) \vec{e}_z, \quad (18)$$

with \vec{e}_z being the unit vector in the vertical direction. A comparison of Eq. (18) with Eq. (8) shows that

$$\alpha = -\frac{1}{k_0} \left(\frac{k_0^2}{Rm} + \frac{d(\ln B_0(t))}{dt} \right) \quad (19)$$

and (up to a spatially constant horizontal field)

$$\vec{\mathcal{E}}_{\perp} = \mathcal{E}_z(z) \vec{e}_z. \quad (20)$$

$\vec{\mathcal{E}}_{\perp}$ is a curl-free field and, thus, not capable of inductive effects. That is, the Roberts dynamo is a pure α -effect dynamo. Eq. (19) shows that

$$\alpha k_0 < 0 \quad (21)$$

is a necessary condition for the growth or maintenance of the mean magnetic field. For a stationary state, in particular, Eq. (19) gives

$$\alpha = -\frac{k_0}{Rm}. \quad (22)$$

In time-dependent final states, the α -effect is temporally modulated by the logarithmic time derivative of the mean-field amplitude. On time average this additional contribution

vanishes. In a kinematic phase of exponential growth at a rate γ , i.e., $\vec{B} \sim e^{\gamma t}$, one gets from Eq. (19)

$$\alpha = -\left(\frac{k_0}{Rm} + \gamma\right). \quad (23)$$

Using Eqs. (8), (17) and (19), Eq. (16) can also be written as

$$\partial_t \langle \vec{B} \rangle = -Rm^{-1} k_0^2 \langle \vec{B} \rangle - k_0 \vec{\mathcal{E}}_{\parallel}. \quad (24)$$

We now prove analytically that, unless the vertical wave number k_0 is restricted to small values, magnetic modes in addition to those belonging to the primary mode triads or, equivalently, to the MTM, with wave vectors $\vec{k} = \vec{k}^{(2)} = (0, 0, \pm k_0)$ and $\vec{k} = \vec{k}^{(3)} = (\pm 1, \pm 1, \pm k_0)$, respectively, must be included into the model in order to enable a dynamo bifurcation from the non-magnetic Roberts flow (cf. Section 2). Assume that only the magnetic modes with $\vec{k} = (0, 0, \pm k_0)$, corresponding to the mean field $\langle \vec{B} \rangle$, and $\vec{k} = (\pm 1, \pm 1, \pm k_0)$, corresponding to the fluctuations \vec{B}' , are included. It is sufficient here to consider the kinematic problem, i.e. the magnetic induction equations (9) and (10) with the velocity field $\vec{u} = \vec{u}' = \vec{u}_R$ (the primary Roberts flow) prescribed. Eq. (10) then becomes

$$\partial_t \vec{B}' = \nabla \times (\vec{u}_R \times \langle \vec{B} \rangle) + Rm^{-1} \nabla^2 \vec{B}' \quad (25)$$

since $\langle \vec{u} \rangle = \vec{0}$ and since no contributions to \vec{G} with the wave vectors $\vec{k} = (\pm 1, \pm 1, \pm k_0)$ admitted for \vec{B}' are obtained from the product of $\vec{u}' = \vec{u}_R$, which corresponds to wave vectors $\vec{k} = (\pm 1, \pm 1, 0)$, with \vec{B}' . The neglect of the term $\nabla \times \vec{G}$ in Eq. (10) is known as first-order smoothing or second-order correlation approximation [3] and is widely employed in dynamo studies. We note that, vice versa, also first-order smoothing just amounts to a restriction to the primary mode triads. Namely,

$$\partial_t \vec{B}'_k = Rm^{-1} \nabla^2 \vec{B}'_k \quad \text{for } \vec{k} \neq (\pm 1, \pm 1, \pm k_0) \quad (26)$$

according to Eq. (25). That is, Fourier components of \vec{B}' not belonging to the primary mode triads, if they should be present initially, are bound to decay under first-order smoothing. Thus, first-order smoothing and the MTM are equivalent approximations.

The time derivative of the turbulent emf, defined by Eq. (8), is given by

$$\begin{aligned} \partial_t \vec{\mathcal{E}} = \langle \vec{u}_R \times \partial_t \vec{B}' \rangle &= \langle \vec{u}_R \times [\nabla \times (\vec{u}_R \times \langle \vec{B} \rangle)] \rangle \\ &+ Rm^{-1} \langle \vec{u}_R \times \nabla^2 \vec{B}' \rangle, \end{aligned} \quad (27)$$

which after some algebra (see Appendix B) and by using

$$\nabla^2 \vec{B}' = -(\pm 1, \pm 1, \pm k_0)^2 \vec{B}' = -(k_0^2 + 2) \vec{B}' \quad (28)$$

becomes

$$\partial_t \vec{\mathcal{E}} = (k_0 - 1) \langle \vec{B} \rangle - Rm^{-1} (k_0^2 + 2) \vec{\mathcal{E}}, \quad (29)$$

the projection of which on the direction of $\langle \vec{B} \rangle$ is

$$\partial_t \vec{\mathcal{E}}_{\parallel} = (k_0 - 1) \langle \vec{B} \rangle - Rm^{-1} (k_0^2 + 2) \vec{\mathcal{E}}_{\parallel} \quad (30)$$

(note that according to Eq. (13), the spatial direction of $\langle \vec{B} \rangle$ is constant in time).

The solutions to the system of Eqs. (24) and (30) are of the form

$$\langle \vec{B} \rangle = \langle \vec{B} \rangle_0 e^{\gamma t}, \quad \vec{\mathcal{E}}_{\parallel} = \langle \vec{\mathcal{E}}_{\parallel} \rangle_0 e^{\gamma t}, \quad (31)$$

with γ determined by the eigenvalue equation

$$\begin{vmatrix} -Rm^{-1} k_0^2 - \gamma & -k_0 \\ k_0 - 1 & -Rm^{-1} (k_0^2 + 2) - \gamma \end{vmatrix} = 0, \quad (32)$$

giving

$$\gamma = -\frac{k_0^2 + 1}{Rm} \pm \frac{1}{Rm} \sqrt{1 + Rm^2 k_0 (1 - k_0)}. \quad (33)$$

Eq. (33) shows that growing magnetic modes are non-oscillatory. Non-decaying magnetic modes exist if and only if

$$1 + Rm^2 k_0 (1 - k_0) \geq (k_0^2 + 1)^2 = k_0^4 + 2k_0^2 + 1, \quad (34)$$

which implies, in particular,

$$0 \leq k_0 < 1 \quad (35)$$

and is equivalent to

$$Rm^2 \geq R_c^2 = \frac{k_0(k_0^2 + 2)}{1 - k_0}. \quad (36)$$

Thus, condition (36) is necessary and sufficient for the existence of a dynamo solution within the frame of the MTM or if, equivalently, first-order smoothing is applied. This analytic condition does not seem to have been found in the kinematic dynamo studies preceding or accompanying the Karlsruhe experiment, which were mostly done within the MTM, as the work of Busse and his coworkers (see, e.g., Refs. [32,35,52]), or by using the equivalent first-order smoothing approximation, as in the investigations of Rädler and his coworkers (see, e.g., Refs. [39,41,45]). In these studies, analytical expressions for the critical magnetic Reynolds number were derived for the limiting case $k_0^2 \ll 1$. Asymptotically in this limit, Eq. (36) gives $R_c^2 \approx 2k_0$, which is in agreement, for instance, with the condition given by Busse in Ref. [52] (Eq. (2.22) in this reference; the choice $\alpha = 1$, $A = 1$, $C = 2$ for the parameters therein corresponds to our model; cf. also Eqs. (18a,b) in Ref. [35]).

From condition (36) it is seen that the dynamo solution ceases to exist as the vertical wave number k_0 approaches the value of 1 from below. By contrast, our numerical calculations for the OTM, i.e. with secondary mode triads (cf. Section 2) taken into account show that there exists a dynamo solution for $0 \leq k_0 < 1$ as well as for $k_0 \geq 1$ and that its properties change continuously as k_0 passes through 1. The special mode interactions that lead to dynamo action for $k_0 \geq 1$ are thus at work also for $k_0 < 1$ and the MTM can be expected to be valid only for sufficiently small values of $|k_0|$.

Then, a look at the actual parameters of the Karlsruhe experiment seems in order. The parameters relevant here are

(i) the diameter of a single spin generator in the array of spin generators (the spin generators correspond to the rolls where the fluid spirals up or down), $a = 0.21$ m, and (ii) the height of the spin generators, $d = 0.703$ m (numbers from Ref. [18]; d is the height of the homogeneous part of the dynamo module, without the connections between different spin generators). Identifying $2a$ with our horizontal period length $L_x = L_y$ (a natural assumption in view of the experimental configuration) and d with the vertical period length L_z (though the actual vertical boundary conditions in the experiment are certainly more complicated than our periodic ones), we get the estimate $k_0 \approx 2a/d = 0.6$ for the experiment. This wave number is not yet very small compared with 1 so that corrections to first-order smoothing or the MTM could also be of practical interest.

6. Conclusions

In this paper, it has been shown that the essential dynamics of a Roberts-type flow configuration in an electrically conducting fluid can be described by truncation models containing only relatively few Fourier modes. The requirement that they have to satisfy all the symmetries of the original problem furnishes them as feasible models for studying symmetry-breaking bifurcations and magnetic field generation. Including successively more interacting mode triads while observing the symmetry requirements, a hierarchy of models is obtained. Also, in each single model there is a hierarchy of mode triads, starting with the primary triads formed by the Roberts flow, a horizontally averaged mean magnetic field and another part of the magnetic field coupled to these two by triadic mode interactions. Two models out of the hierarchy, the MTM and the OTM, were chosen for a detailed consideration.

In Section 5, it has been shown that the MTM, containing only the modes of the primary triads, is fully equivalent to the first-order smoothing approximation of mean-field theory. The Roberts dynamo is a pure α -effect dynamo with a purely horizontal α -effect. This can be treated largely analytically, leading, e.g., to a simple dependence of the α -effect parameter α on the magnetic Reynolds number for stationary dynamo solutions. For the MTM, a simple analytic condition could be derived giving the critical magnetic Reynolds number for the onset of dynamo action as a function of the vertical wave number k_0 of the magnetic field (with the wave numbers of the flow in the horizontal directions x and y fixed to the value of 1). The condition shows, e.g., that the MTM is invalid for vertical wave numbers k_0 close to or larger than 1. This could be of practical interest for the Karlsruhe dynamo experiment since the wave number k_0 there, though smaller than 1, is not small compared with 1. In order to overcome the restriction to small vertical wave numbers, we have chosen the more general OTM as a representative model by means of which we then have investigated the dynamo solutions in more detail from the viewpoint of nonlinear dynamics. Especially, the symmetry breaking bifurcations on the route to chaos have been studied and classified.

The dominating role of the $S^1 \times Z_2$ subsymmetry, corresponding to the translational symmetry of the Roberts

flow combined with the reflection symmetry, $\vec{v} \rightarrow \vec{v}$ and $\vec{B} \rightarrow -\vec{B}$, of the induction equation, has been elucidated. It is responsible for the generation of OW in the transition to the time-periodic regime. The OW branch is characterised by a surviving spatio-temporal Z_2 invariance of the periodic orbit. A further bifurcation within the time-periodic regime has been detected, with the bifurcating branch denoted as OW*. The solutions of this branch still possess the spatio-temporal Z_2 symmetry. However, they can be clearly distinguished from the OW by the form and temporal behaviour of the mean magnetic field leading, in particular, to a reduced dynamo activity. Last but not least, the occurrence of a finite interval of Re appears remarkable where, compared to a preceding normal torus solution, there exists an additional marginal direction in phase space and, thus, four Lyapunov exponents are equal to zero, before chaos then sets in. We suppose that this special torus-chaos transition is also generically caused by the $S^1 \times Z_2$ symmetry.

Acknowledgements

The authors thank K.-H. Rädler and M. Rheinhardt for helpful discussions on the validity limits of the first-order smoothing approximation in mean-field theory.

Appendix A. Derivation of the OTM

In order to derive a truncation model from the MHD equations, Eqs. (1)–(3), we use Fourier ansatzes for \vec{v} , \vec{B} and p . Periodic boundary conditions are imposed on the domain $\Omega = [L_x \times L_y \times L_z]$, where the mean values of the variables in Ω are assumed to vanish. As in [63,64], the solutions are expanded into the complete set of orthogonal eigenfunctions of the Stokes operator, i.e.

$$\vec{u}(\vec{x}) = \sum_{\vec{k} \neq \vec{0}} \left(u_{\vec{k}}^{(1)} \vec{e}_{\vec{k}}^{(1)} + u_{\vec{k}}^{(2)} \vec{e}_{\vec{k}}^{(2)} \right) \exp(i\vec{k} \cdot \vec{x}), \quad (\text{A.1})$$

$$\vec{B}(\vec{x}) = \sum_{\vec{k} \neq \vec{0}} \left(B_{\vec{k}}^{(1)} \vec{e}_{\vec{k}}^{(1)} + B_{\vec{k}}^{(2)} \vec{e}_{\vec{k}}^{(2)} \right) \exp(i\vec{k} \cdot \vec{x}), \quad (\text{A.2})$$

$$p(\vec{x}) = \sum_{\vec{k} \neq \vec{0}} p_{\vec{k}} \exp(i\vec{k} \cdot \vec{x}), \quad (\text{A.3})$$

where we have used real polarization vectors $\vec{e}_{\vec{k}}^{(1)}$, $\vec{e}_{\vec{k}}^{(2)}$ perpendicular to \vec{k} , satisfying

$$\vec{e}_{\vec{k}}^{(i)} \cdot \vec{k} = 0, \quad \vec{e}_{\vec{k}}^{(1)} \cdot \vec{e}_{\vec{k}}^{(2)} = 0, \quad \vec{e}_{\vec{k}}^{(i)} \cdot \vec{e}_{\vec{k}}^{(i)} = 1, \quad \vec{e}_{-\vec{k}}^{(i)} = \vec{e}_{\vec{k}}^{(i)} \quad (\text{A.4})$$

for $i = 1, 2$,

such that Eqs. (3) are satisfied automatically. Because of the last condition in Eq. (A.4) we have

$$u_{-\vec{k}}^{(i)} = \left(u_{\vec{k}}^{(i)} \right)^*, \quad B_{-\vec{k}}^{(i)} = \left(B_{\vec{k}}^{(i)} \right)^* \quad (\text{A.5})$$

(an asterisk indicates the complex conjugate). By means of the above Fourier expansions, Eqs. (A.1)–(A.3), we get rid of the

pressure term in Eq. (1) and arrive at the following system of ordinary differential equations (ODEs):

$$\frac{du_{\vec{k}}^{(j)}}{dt} = -i \sum_{\vec{q} \neq \{0, \pm \vec{k}\}} \sum_{m,n=1}^2 \left(\vec{e}_{\vec{q}}^{(n)} \cdot \vec{e}_{\vec{k}}^{(j)} \right) \left(\vec{e}_{\vec{k}-\vec{q}}^{(m)} \cdot \vec{k} \right) \times \left(u_{\vec{q}}^{(n)} u_{\vec{k}-\vec{q}}^{(m)} - B_{\vec{q}}^{(n)} B_{\vec{k}-\vec{q}}^{(m)} \right) - \frac{\vec{k}^2}{Re} u_{\vec{k}}^{(j)} + f_{\vec{k}}^{(j)} \quad (\text{A.6})$$

$$\frac{dB_{\vec{k}}^{(j)}}{dt} = -i \sum_{\vec{q} \neq \{0, \pm \vec{k}\}} \sum_{m,n=1}^2 \left(\vec{e}_{\vec{q}}^{(n)} \cdot \vec{e}_{\vec{k}}^{(j)} \right) \left(\vec{e}_{\vec{k}-\vec{q}}^{(m)} \cdot \vec{k} \right) \times \left(B_{\vec{q}}^{(n)} u_{\vec{k}-\vec{q}}^{(m)} - u_{\vec{q}}^{(n)} B_{\vec{k}-\vec{q}}^{(m)} \right) - \frac{\vec{k}^2}{Rm} B_{\vec{k}}^{(j)}. \quad (\text{A.7})$$

Now all modes that do not belong to the primary or secondary mode triads depicted in Fig. 2 are neglected. Taking into account the conditions in Eq. (A.5), this leads to 152 (=19 · 8) ODEs for the real and imaginary parts of the complex mode coefficients $u_{\vec{k}}^{(j)}$ and $B_{\vec{k}}^{(j)}$ making up the model (OTM) studied in the present paper.

Appendix B. Algebraic relations for Section 5

The time derivative of the turbulent emf, defined by Eq. (8), is given by

$$\partial_t \vec{\mathcal{E}} = \left\langle \vec{u}_R \times \partial_t \vec{B}' \right\rangle = \left\langle \vec{u}_R \times \left[\nabla \times \left(\vec{u}_R \times \left\langle \vec{B} \right\rangle \right) \right] \right\rangle + Rm^{-1} \left\langle \vec{u}_R \times \nabla^2 \vec{B}' \right\rangle. \quad (\text{B.1})$$

Using Eqs. (4) and (13), one finds for the first term on the right-hand side of Eq. (B.1)

$$\nabla \times \left(\vec{u}_R \times \left\langle \vec{B} \right\rangle \right) = B_0 \times \begin{pmatrix} (2k_0 - 1) \sin x \sin y \sin(k_0 z) + \cos x \cos y \cos(k_0 z) \\ -(2k_0 - 1) \sin x \sin y \cos(k_0 z) - \cos x \cos y \sin(k_0 z) \\ 2 \cos x \sin y \cos(k_0 z) + 2 \sin x \cos y \sin(k_0 z) \end{pmatrix} \quad (\text{B.2})$$

and further

$$\vec{u}_R \times \left[\nabla \times \left(\vec{u}_R \times \left\langle \vec{B} \right\rangle \right) \right] = B_0 \times \begin{pmatrix} 2(2k_0 \sin^2 x - 1) \sin^2 y \cos(k_0 z) \\ 2 \sin^2 x (2k_0 \sin^2 y - 1) \sin(k_0 z) \\ \frac{1}{2} \left[(1 - 2k_0 \sin^2 x) \sin(2y) \cos(k_0 z) - \sin(2x) (1 - 2k_0 \sin^2 y) \sin(k_0 z) \right] \end{pmatrix} \quad (\text{B.3})$$

which on horizontal averaging gives

$$\left\langle \vec{u}_R \times \left[\nabla \times \left(\vec{u}_R \times \left\langle \vec{B} \right\rangle \right) \right] \right\rangle = B_0 \begin{pmatrix} (k_0 - 1) \cos(k_0 z) \\ (k_0 - 1) \sin(k_0 z) \\ 0 \end{pmatrix} = (k_0 - 1) \left\langle \vec{B} \right\rangle. \quad (\text{B.4})$$

References

[1] H.K. Moffatt, *Magnetic Field Generation in Electrically Conducting Fluids*, Cambridge University Press, Cambridge, 1978.

[2] E.N. Parker, *Cosmical Magnetic Fields*, Clarendon Press, Oxford, 1979.
 [3] F. Krause, K.-H. Rädler, *Mean-Field Magnetohydrodynamics and Dynamo Theory*, Akademie-Verlag, Berlin, 1980.
 [4] Y. Zeldovich, A.A. Ruzmaikin, D.D. Sokoloff, *Magnetic Fields in Astrophysics*, Gordon and Breach, New York, 1983.
 [5] P.H. Roberts, G.A. Glatzmaier, *Geodynamo theory and simulations*, *Rev. Modern Phys.* 72 (2000) 1081–1123.
 [6] K.-H. Rädler, The generation of cosmic magnetic fields, in: D. Page, J.G. Hirsch (Eds.), *From the Sun to the Great Attractor: 1999 Guanajuato Lectures on Astrophysics*, in: *Lecture Notes in Physics*, vol. 556, Springer, New York, 2000, pp. 101–172.
 [7] A.D. Gilbert, *Dynamo theory*, in: S.J. Friedlander, D. Serre (Eds.), *Handbook of Mathematical Fluid Dynamics*, vol. 2, Elsevier, Amsterdam, 2003, pp. 355–441.
 [8] J. Larmor, How could a rotating body such as the Sun become a magnet? *Rep. Brit. Assoc. Adv. Sci.* (1919) 159–160.
 [9] A. Gailitis, O. Lielausis, S. Dement'ev, E. Platācis, A. Ciferons, G. Gerbeth, T. Gundrum, F. Stefani, M. Christen, H. Hänel, G. Will, Detection of a flow induced magnetic field eigenmode in the Riga dynamo facility, *Phys. Rev. Lett.* 84 (2000) 4365–4368.
 [10] A. Gailitis, O. Lielausis, E. Platācis, S. Dement'ev, A. Ciferons, G. Gerbeth, T. Gundrum, F. Stefani, M. Christen, G. Will, Magnetic field saturation in the Riga dynamo experiment, *Phys. Rev. Lett.* 86 (2001) 3024–3027.
 [11] A. Gailitis, O. Lielausis, E. Platācis, G. Gerbeth, F. Stefani, Riga dynamo experiment, in: P. Chossat, D. Armbruster, I. Oprea (Eds.), *Dynamo and Dynamics, a Mathematical Challenge*, in: *NATO Science Series II: Mathematics, Physics and Chemistry*, vol. 26, Kluwer, Dordrecht, 2001, pp. 9–16.
 [12] A. Gailitis, O. Lielausis, E. Platācis, G. Gerbeth, F. Stefani, On the results of the Riga dynamo experiments, *Magnetohydrodynamics* 37 (2001) 71–79.
 [13] A. Gailitis, O. Lielausis, E. Platācis, S. Dement'ev, A. Ciferons, G. Gerbeth, T. Gundrum, F. Stefani, M. Christen, G. Will, Dynamo experiments at the Riga sodium facility, *Magnetohydrodynamics* 38 (2002) 5–14.
 [14] A. Gailitis, O. Lielausis, E. Platācis, G. Gerbeth, F. Stefani, On back-reaction effects in the Riga dynamo experiment, *Magnetohydrodynamics* 38 (2002) 15–26.
 [15] A. Gailitis, O. Lielausis, E. Platācis, G. Gerbeth, F. Stefani, The Riga dynamo experiment, *Surv. Geophys.* 24 (2003) 247–267.
 [16] R. Stieglitz, U. Müller, *GEODYNAMO — Eine Versuchsanlage zum Nachweis des homogenen Dynamoeffektes*, Research Report FZKA-5716, Forschungszentrum Karlsruhe, 1996.
 [17] U. Müller, R. Stieglitz, Can the Earth's magnetic field be simulated in the laboratory? *Naturwiss.* 87 (2000) 381–390.
 [18] R. Stieglitz, U. Müller, Experimental demonstration of a homogeneous two-scale dynamo, *Phys. Fluids* 13 (2001) 561–564.
 [19] U. Müller, R. Stieglitz, The Karlsruhe dynamo experiment, *Nonlin. Proc. Geophys.* 9 (2002) 165–170.
 [20] R. Stieglitz, U. Müller, Experimental demonstration of a homogeneous two-scale dynamo, *Magnetohydrodynamics* 38 (2002) 27–33.
 [21] U. Müller, R. Stieglitz, S. Horanyi, A two-scale hydromagnetic dynamo experiment, *J. Fluid Mech.* 498 (2004) 31–71.
 [22] F.H. Busse, Homogeneous dynamos in planetary cores and in the laboratory, *Annu. Rev. Fluid Mech.* 32 (2000) 383–408.
 [23] A. Tilgner, Towards experimental fluid dynamos, *Phys. Earth Planet. Inter.* 117 (2000) 171–177.
 [24] A. Tilgner, Laboratory dynamo experiments and what we learned from them, *Astron. Nachr.* 323 (2002) 407–410.
 [25] A. Gailitis, O. Lielausis, E. Platācis, G. Gerbeth, F. Stefani, Laboratory experiments on hydromagnetic dynamos, *Rev. Modern Phys.* 74 (2002) 973–990.
 [26] G.O. Roberts, Spatially periodic dynamos, *Phil. Trans. R. Soc. Lond. A* 266 (1970) 535–558.
 [27] G.O. Roberts, Dynamo action of fluid motions with two-dimensional

- periodicity, *Phil. Trans. R. Soc. Lond. A* 271 (1972) 411–454.
- [28] F.H. Busse, A simple model of convection in the Jovian atmosphere, *Icarus* 29 (1976) 255–260.
- [29] F.H. Busse, Convection driven zonal flows and vortices in the major planets, *Chaos* 4 (1994) 123–134.
- [30] A.P. Ingersoll, D. Pollard, Motion in the interiors and atmospheres of Jupiter and Saturn: scale analysis, anelastic equations, barotropic stability criterion, *Icarus* 52 (1982) 62–80.
- [31] F.H. Busse, A model of the geodynamo, *Geophys. J. Roy. Astron. Soc.* 42 (1975) 437–459.
- [32] F.H. Busse, Dynamo theory of planetary magnetism and laboratory experiments, in: R. Friedrich, A. Wunderlin (Eds.), *Evolution of Dynamical Structures in Complex Systems*, in: Springer Proceedings in Physics, vol. 69, Springer, Berlin, 1992, pp. 197–208.
- [33] F.H. Busse, U. Müller, R. Stieglitz, A. Tilgner, A two-scale homogeneous dynamo. An extended analytical model and an experimental demonstration under development, *Magnetohydrodynamics* 32 (1996) 259–271.
- [34] A. Tilgner, A kinematic dynamo with a small scale velocity field, *Phys. Lett. A* 226 (1997) 75–79.
- [35] F.H. Busse, U. Müller, R. Stieglitz, A. Tilgner, Spontaneous generation of magnetic fields in the laboratory, in: F.H. Busse, S.C. Müller (Eds.), *Evolution of Spontaneous Structures in Dissipative Continuous Systems*, in: Lecture Notes in Physics, vol. m 55, Springer, Berlin, 1998, pp. 546–558.
- [36] A. Tilgner, F.H. Busse, Saturation mechanism in a model of the Karlsruhe dynamo, in: P. Chossat, D. Armbruster, I. Oprea (Eds.), *Dynamo and Dynamics, a Mathematical Challenge*, in: NATO Science Series II: Mathematics, Physics and Chemistry, vol. 26, Kluwer, Dordrecht, 2001, pp. 109–116.
- [37] A. Tilgner, F.H. Busse, Simulation of the bifurcation diagram of the Karlsruhe dynamo, *Magnetohydrodynamics* 38 (2002) 35–40.
- [38] A. Tilgner, Numerical simulation of the onset of dynamo action in an experimental two-scale dynamo, *Phys. Fluids* 14 (2002) 4092–4094.
- [39] A. Apel, E. Apstein, K.-H. Rädler, M. Rheinhardt, Contributions to the theory of the Karlsruhe dynamo experiment, Research Report, Astrophysikalisches Institut Potsdam, 1996.
- [40] K.-H. Rädler, E. Apstein, M. Rheinhardt, M. Schüler, The Karlsruhe dynamo experiment. A mean-field approach, *Stud. Geophys. Geod.* 42 (3) (1998) 224–231.
- [41] K.-H. Rädler, M. Rheinhardt, E. Apstein, H. Fuchs, On the mean-field theory of the Karlsruhe dynamo experiment I. Kinematic theory, *Magnetohydrodynamics* 38 (2002) 41–71.
- [42] K.-H. Rädler, M. Rheinhardt, E. Apstein, H. Fuchs, On the mean-field theory of the Karlsruhe dynamo experiment II. Back-reaction of the magnetic field on the fluid flow, *Magnetohydrodynamics* 38 (2002) 73–94.
- [43] F. Plunian, K.-H. Rädler, Subharmonic dynamo action in the Roberts flow, *Geophys. Astrophys. Fluid Dyn.* 96 (2002) 115–133.
- [44] F. Plunian, K.-H. Rädler, Harmonic and subharmonic solutions of the Roberts dynamo problem. Application to the Karlsruhe experiment, *Magnetohydrodynamics* 38 (2002) 95–106.
- [45] K.-H. Rädler, A. Brandenburg, Contributions to the theory of a two-scale homogeneous dynamo experiment, *Phys. Rev. E* 67 (2003) 026401.
- [46] S. Rüdiger, F. Feudel, N. Seehafer, Dynamo bifurcations in an array of driven convectionlike rolls, *Phys. Rev. E* 57 (1998) 5533–5538.
- [47] F. Feudel, M. Gellert, S. Rüdiger, A. Witt, N. Seehafer, Dynamo effect in a driven helical flow, *Phys. Rev. E* 68 (2003) 046302.
- [48] P.D. Mininni, D.C. Montgomery, Low magnetic Prandtl number dynamos with helical forcing, *Phys. Rev. E* 72 (2005) 056320.
- [49] E.N. Lorenz, Deterministic non-periodic flow, *J. Atmos. Sci.* 20 (1963) 130–141.
- [50] V. Franceschini, C. Giberti, M. Nicolini, Common periodic behaviour in larger and larger truncations of the Navier–Stokes equations, *J. Stat. Phys.* 50 (1988) 879–896.
- [51] A. Witt, R. Braun, F. Feudel, C. Grebogi, J. Kurths, Tracer dynamics in a flow of driven vortices, *Phys. Rev. E* 59 (1999) 1605–1614.
- [52] F.H. Busse, Magnetohydrodynamics of the earth’s dynamo, *Ann. Rev. Fluid Mech.* 10 (1978) 435–462.
- [53] A. Kageyama, T. Sato, Dynamo efficiency and Beltrami flows in rectangular cells, *Phys. Plasmas* 6 (1999) 771–776.
- [54] A.M. Soward, Fast dynamo action in a steady flow, *J. Fluid Mech.* 180 (1987) 267–295.
- [55] A.M. Soward, On dynamo action in a steady flow at large magnetic Reynolds number, *Geophys. Astrophys. Fluid Dyn.* 49 (1989) 3–22.
- [56] A.M. Soward, Fast dynamos, in: M.R.E. Proctor, A.D. Gilbert (Eds.), *Lectures on Solar and Planetary Dynamos*, Cambridge University Press, Cambridge, 1994, pp. 181–217.
- [57] A.S. Landsberg, E. Knobloch, Direction-reversing traveling waves, *Phys. Lett. A* 159 (1991) 17–20.
- [58] F. Amdjadi, J. Gomatam, Oscillating waves arising from $O(2)$ symmetry, *Phys. Lett. A* 231 (1997) 379–388.
- [59] F. Amdjadi, P.J. Aston, P. Plecháč, Symmetry breaking Hopf bifurcations in equations with $O(2)$ symmetry, *J. Comput. Phys.* 131 (1997) 181–192.
- [60] A. Sarkar, A. Tilgner, Magnetic field oscillations in the Karlsruhe dynamo, *Astron. Nachr.* 326 (2005) 250–253.
- [61] P.H. Roberts, A.M. Soward, Dynamo theory, *Annu. Rev. Fluid Mech.* 24 (1992) 459–512.
- [62] N. Seehafer, M. Gellert, K.M. Kuzanyan, V.V. Pipin, Helicity and the solar dynamo, *Adv. Space Res.* 32 (10) (2003) 1819–1833.
- [63] F. Feudel, N. Seehafer, B. Galanti, S. Rüdiger, Symmetry-breaking bifurcations for the magnetohydrodynamic equations with helical forcing, *Phys. Rev. E* 54 (1996) 2589–2596.
- [64] N. Seehafer, F. Feudel, O. Schmidtman, Nonlinear dynamo with ABC forcing, *Astron. Astrophys.* 314 (1996) 693–699.